Satellite and Correlative Measurements of the Stratospheric Aerosol. III: Comparison of Measurements by SAM II, SAGE, Dustsondes, Filters, Impactors and Lidar

P. B. RUSSELL

NASA Ames Research Center, Moffett Field, CA 94035

M. P. MCCORMICK

NASA Langley Research Center, Hampton, VA 23665

T. J. SWISSLER

Systems and Applied Sciences Corporation, Hampton, VA 23666

J. M. ROSEN AND D. J. HOFMANN

Department of Physics and Astronomy, University of Wyoming Laramie, WY 82070

L. R. MCMASTER

NASA Langley Research Center, Hampton, VA 23665

(Manuscript received 10 August 1983, in final form 30 March 1984)

ABSTRACT

A large satellite validation experiment was conducted at Poker Flat, Alaska, 16–19 July 1979. Instruments included the SAM II and SAGE satellite sensors, dustsondes, impactors, a filter collector and an airborne lidar. We show that the extinction profiles that were measured independently by SAM II and SAGE agree with each other. We then use a generalized optical model (which agrees with the Poker Flat optical absorption and relative size distribution measurements) to derive extinction profiles from the other measurements. Extinction profiles thus derived from the dustsonde, filter and lidar measurements agree with the satellite-measured extinction profiles to within the combined uncertainties. (Individual 1 σ uncertainties are, at most heights, roughly 7 to 20% each for the satellite, dustsonde and filter measurements, 30 to 60% for the lidar measurements, and 10 to 20% for the process of converting one measured parameter to another using the optical model.)

The wire impactor-derived results are also consistent with the other results, but the comparison is coarse because of the relatively large uncertainties (±35% to a factor of 4) in impactor-derived mass, extinction, $N_{0.15}$ and $N_{0.25}$. (N_x is the number of particles per unit volume with radius greater than x μm.) These uncertainties apply to background stratospheric aerosol size distributions, and result primarily from relatively small uncertainties (±8 to ±20% for confidence limits of 95%) in radii assigned to impacted particles, combined with the steepness of background size distributions in the radius range that contributes most to mass, extinction, $N_{0.15}$ and $N_{0.25}$. Polar nephelometer-measured asymmetry parameters (0.4 to 0.6) agree with a previous balloon photometer inference, but are significantly less than the value (~0.7) obtained from Mie scattering calculations assuming either model or measured size distributions.

1. Introduction

The previous two papers in this series (Russell *et al.*, 1981a,b, henceforth called Papers I and II) described a generalized stratospheric aerosol optical model and used it to compare measurements made by the satellite sensor Stratospheric Aerosol Measurement II (SAM II), dustsondes, and an airborne lidar in an experiment conducted near Sondrestrom, Greenland, in November 1978. After that experiment, the Stratospheric Aerosol and Gas Experiment (SAGE) satellite sensor of stratospheric aerosols, ozone, and nitrogen dioxide was launched (McCormick *et al.*, 1979). A larger experiment was conducted in July 1979 near Poker Flat, Alaska, to compare SAM II and SAGE measurements with each other and with a variety of other sensors. This paper is concerned with aerosol results from Poker Flat; the ozone and NO_2 results are the subject of other papers.

Table 1 lists the aerosol sensors that were used in the Poker Flat experiment. Results from some aerosol sensors (SAM II, integrating plate, polar nephelometer, wire impactor, and multifilter sampler), with some initial comparisons and analyses, have been presented by a collection of short papers in *Geophysical Research*

TABLE 1. Aerosol sensors used in the July 1979 Poker Flat, Alaska, comparative experiment.

Sensor	Particle parameter	Data height (km)	Platform	Investigator
SAM II	Extinction (λ = 1.0 μm)	Cloud tops to 40	Nimbus 7 satellite	McCormick *et al.*
SAGE	Extinction (λ = 1.0 μm)	Cloud tops to 40	AEM-2 satellite	McCormick *et al.*
Dustsonde	Number ($r > 0.15, 0.25$ μm)*	0–29	Balloon	Rosen and Hofmann
Lidar	Backscatter (λ = 0.69 μm)	12–30	P-3 aircraft	Fuller *et al.*
Multifilter sampler	Sulfate mass	12–21	U-2 aircraft	Gandrud and Lazrus
Wire impactor	Number, mass distribution	12–20	U-2 aircraft	Farlow *et al.*
Cascade microbalance (QCM)	Mass, number distribution	12–21	U-2 and Sabreliner aircraft	Woods and Chuan
Integrating plate	Absorption ($\lambda \approx 0.55$ μm)	15–20	U-2 aircraft	Ogren *et al.*
Polar nephelometer	Scattering angular distribution	11–13	Sabreliner aircraft	Grams

Letters (McCormick *et al.*, 1981; Ogren *et al.*, 1981; Grams, 1981; Farlow *et al.*, 1981; Oberbeck *et al.*, 1981; Gandrud and Lazrus, 1981; Toon *et al.*, 1981; Pollack *et al.*, 1981). The purpose of this paper is to validate the SAGE sensor by presenting the (previously unpublished) SAGE, dustsonde, and airborne lidar data, and systematically comparing them with the data from the other sensors.

The comparisons in this paper make use of the generalized optical modeling procedure developed and used in Papers I and II, with the updated refractive index set of Russell and Hamill (1984). Figure 1 shows a schematic representation of the updated model. In brief, the refractive index set of Russell and Hamill takes into account:

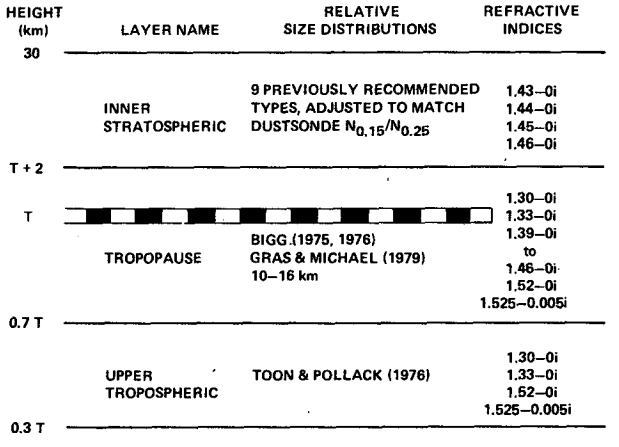

FIG. 1. Vertical structure of model optical properties. T is tropopause height. Inner stratospheric and tropopause-layer refractive indices are as derived by Russell and Hamill (1984).

1) The finding of Hayes *et al.* (1980) that solid ammonium sulfate is evidently not present in background stratospheric aerosols.

2) The method of Steele and Hamill (1981) for computing the effects of stratospheric temperature and humidity on sulfuric acid/water aerosol composition and refractive index. (See also Yue and Deepak, 1981.) The refractive index set of Fig. 1 and Russell and Hamill (1984) has also been used successfully in the 7-year comparison of lidar and dustsonde results made by Swissler *et al.* (1982). As Russell and Hamill note, the new refractive index set yields conversion ratios (e.g., extinction-to-number, backscatter-to-mass) nearly identical to those of Papers I and II, because the refractive index changes (deleting the ammonium sulfate value and increasing the sulfuric acid/water values) have nearly opposite effects on all conversion ratios of interest.

The Poker Flat data set (Table 1) includes measurements of aerosol optical absorption and of size distribution, each of which can be tested for consistency with the optical model. The Appendix includes such a consistency check and also compares the model conversion ratios (in particular, extinction-to-volume and backscatter-to-volume) with the size distribution-independent approximations of Pinnick *et al.* (1980). The Appendix shows that, when the experimental uncertainties of the Poker Flat absorption and wire impactor size distribution measurements are taken into account, the measurements and the model are consistent (including the modeling procedure of parameterizing size distributions in terms of dustsonde channel ratio—i.e., $N_{0.15}/N_{0.25}$, where N_x is the number of particles with radius larger than x μm). Also, the

Pinnick *et al.* approximation for the backscatter-to-volume ratio at a wavelength of 0.69 μm is shown to be consistent with the model (to ±20%); however, the Pinnick *et al.* approximation for the extinction-to-volume ratio at a wavelength of 1.0 μm is somewhat too large for typical background stratospheric aerosol size distributions, for the reasons explained in the Appendix.

2. Data profiles and comparisons

a. SAM II and SAGE

Figure 2 shows the profiles of particulate extinction measured by SAM II and SAGE near Poker Flat on 16, 17, and 19 July 1979. (Data from 18 July were not captured because of telemetry problems). Error bars were computed as described in Paper II. The SAM II profiles differ somewhat from those shown by McCormick *et al.* (1981); those profiles were affected by a small height-scale error caused by a long-term drift in the SAM II scan mirror rate. This drift is now known and properly taken into account. Between 10 and 19 km the current profiles differ from the old ones by less than error bars; however, above 19 km the current SAM II profiles significantly exceed the old ones.

It can be seen that the SAM II and SAGE profiles in Fig. 2 agree within error bars with but one exception. The exception is in Fig. 2c for 19 July near the tropopause. Here, however, there is a very high probability that tropospheric cloud tops could interfere with one satellite sensor and not the other since their individual satellite-sun vectors are not the same, and the measurements are not perfectly simultaneous. (Temporal and horizontal distances between the SAM II and SAGE measurements at Poker Flat differed from day to day, but were of order 30 min and 100 km, respectively.)

In viewing the agreement in Fig. 2, the independent nature of the two satellite measurements should be emphasized. The SAM II and SAGE sensors fly on separate spacecraft (Nimbus 7 and AEM-2, respectively) in different orbits, and thus had considerably different viewing geometries at Poker Flat. Moreover, the sensors themselves differ significantly in optical design and in data handling hardware and software. Thus, agreement between the SAM II and SAGE results was by no means automatic, and was in fact a primary objective of the Poker Flat experiment. The agreement in Fig. 2 shows that this primary objective was realized.

b. Dustsondes

The University of Wyoming dustsondes were flown on 16 and 17 July. Results for $N_{0.15}$ and $N_{0.25}$ are shown in Fig. 3, and results for channel ratio, $N_{0.15}/N_{0.25}$ are shown in Fig. 4. Error bars were derived as shown in Paper II. Points labeled "AWI" are described in Section d below.

c. Multifilter sampler

Figure 5 shows profiles of sulfate mass concentration (open squares) derived from the National Center for Atmospheric Research (NCAR) multifilter sampler as described by Gandrud and Lazrus (1981). The sulfate error bars of ±15% include uncertainties in both flow rate (hence sample air volume) and sample sulfate mass (Gandrud, personal communication, 1981).

We have converted these sulfate mass profiles to profiles of total particle mass assuming a particle composition of sulfuric acid and water. This assumption yields

$$M_p(z) = \frac{1.021 M_s(z)}{W(z)/100\%}, \qquad (1)$$

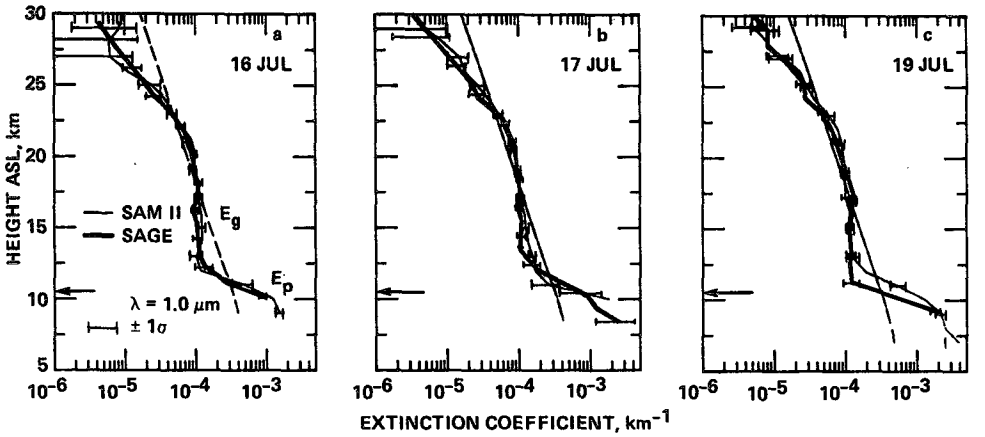

FIG. 2. Particle extinction profiles E_p, measured by SAM II and SAGE during the Poker Flat experiment. The gas extinction coefficient E_g is calculated from radiosonde data. Arrows mark tropopause height.

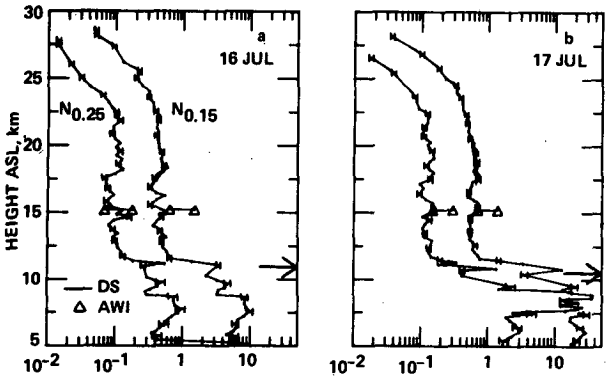

FIG. 3. Particle number density profiles measured by dustsonde (DS) and Ames wire impactor (AWI) during the Poker Flat experiment. For each horizontal pair of AWI data points, the point on the left results from reducing all particle radii by 15%. Arrows mark tropopause height.

where z is altitude, M_p is particle mass, M_s is sulfate mass, and W is particle acid weight percentage. We computed profiles of W using temperature profiles measured at Poker Flat and the model water vapor profiles and method of Russell and Hamill (1984; see e.g., their Fig. 1d). Within the height range of the filter mass measurements, resulting W values ranged from 74% at 13 km to 78% at 20 km with a $\pm 1\sigma$ uncertainty range (caused mainly by water vapor uncertainties) of about ± 3 percentage points at each height. Substituting these values in Eq. (1) yields the total mass concentration profiles (solid squares) in Fig. 5. Error bars include the uncertainty in both M_s and W, combined by standard methods (e.g., Paper II; Bevington, 1969). The error bars (roughly $\pm 16\%$) are nearly impossible to see because they are smaller than the data symbols.

d. Ames wire impactor

Relative size distributions derived from the Ames Wire Impactor (AWI) are shown in Fig. A1. (The absolute distributions are shown in Fig. 1 of Farlow *et al.*, 1981). In this paper we do not use AWI data from the upper sampling altitudes (18.3 and 19.8 km). Samples collected at those altitudes were highly unusual, with droplets appearing to be much less viscous than normal; they were unusually flattened on the wire, thus making size determinations difficult. Farlow *et al.* (1981) did not use the 18.3–19.8 km samples for comparisons and we follow that practice here.

Integrating the absolute AWI size distributions yields the $N_{0.15}$, $N_{0.25}$, and $N_{0.15}/N_{0.25}$ values shown in Figs. 3 and 4. These values are almost identical to those in Table 1 of Farlow *et al.* (1981) with the exception of some values which differ slightly but not significantly, evidently because our size distribution curves (Fig. A1) pass exactly through each data point, whereas the curves of Farlow *et al.* (their Fig. 1) are slightly smoothed. As noted by Farlow *et al.*, the $N_{0.15}$ and $N_{0.25}$ values derived from the AWI unshifted size distributions considerably exceed the dustsonde-derived values for most heights and dates. They also noted that this discrepancy might be caused by the assignment of AWI particle counts to radii that are somewhat too large. (Confidence limits of 95% on AWI-inferred radii are about $\pm 8\%$ to $\pm 20\%$, with the largest uncertainties applying to the largest and smallest radii. See Fig. 1 of Farlow *et al.*, and Fig. 1 of Oberbeck *et al.*, 1981.) Therefore, we also show in Figs. 3 and 4, AWI results for distributions shifted in radius by -15%. This comparison emphasizes the sensitivity of $N_{0.15}$ and $N_{0.25}$ to small radius shifts: $N_{0.15}$ and $N_{0.25}$ decrease by nearly a factor of 2. Such shifts improve the agreement between dustsonde and AWI $N_{0.15}$ and $N_{0.25}$ values.

Figure 4 shows that AWI-inferred channel ratios, $N_{0.15}/N_{0.25}$, are not very sensitive to radius shifts. For 17 July at 15.2 km, both shifted and unshifted AWI distributions yield $N_{0.15}/N_{0.25} \approx 5$, in good agreement with the dustsonde value. However, on 16 July at 15.2 km, both shifted and unshifted AWI distributions are steeper, yielding $N_{0.15}/N_{0.25} \approx 8$; this is significantly larger than the dustsonde value.

We have also converted the AWI size distributions to mass values using droplet specific gravity profiles computed in analogy to the acid weight percentage profiles described in Section 3.c. (Specific gravity ranged from 1.65 at 12 km to 1.76 at 20 km, with a $\pm 1\sigma$ uncertainty of ± 0.03 at each height. Compare Fig. 1e of Russell and Hamill, 1984.) Resulting values, for both shifted and unshifted AWI distributions, are compared to the NCAR filter values in Fig. 5. This comparison shows that, for the background stratospheric aerosol conditions in this experiment, the AWI-inferred mass values are extremely sensitive to small radius shifts—changes in mass by a factor of 3 or more are not uncommon for the -15% radius shift. In gen-

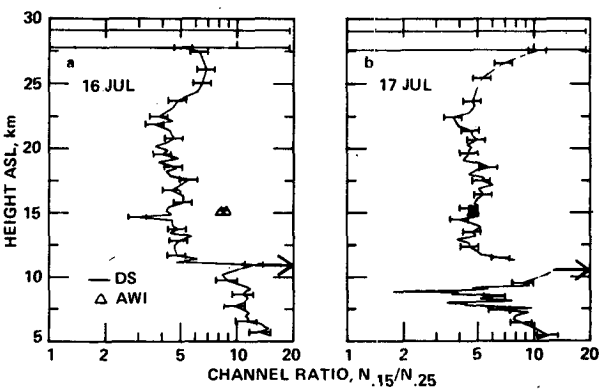

FIG. 4. Channel ratio profiles measured by dustsonde (DS) and Ames wire impactor (AWI) during the Poker Flat experiment. For each horizontal pair of AWI data points, the point on the right results from reducing all particle radii by 15%. Arrows mark tropopause height.

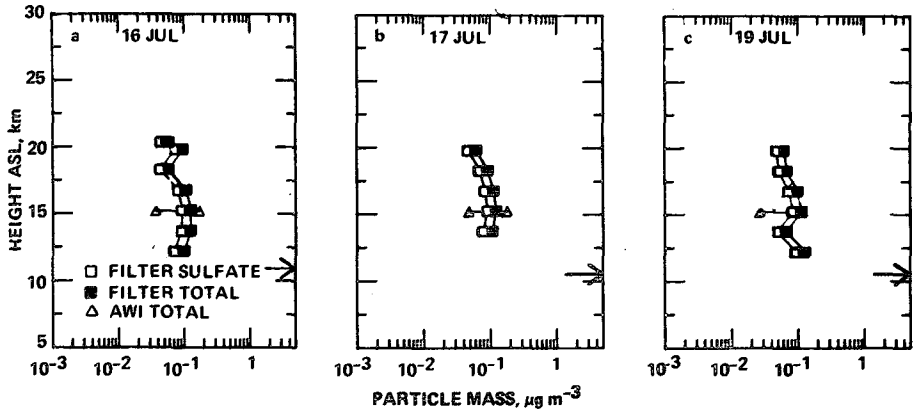

FIG. 5. Sulfate and total particle mass profiles measured by NCAR filter and Ames wire impactor (AWI) during the Poker Flat experiment. For each horizontal pair of AWI data points, the point on the left results from reducing all particle radii by 15%. Arrows mark tropopause height.

eral, the unshifted AWI masses exceed those measured by the filter, whereas a −15% radius shift more than compensates for the mass discrepancy.

e. Lidar

Because of the transmit-receive alignment problems, valid lidar data were obtained only on 19 July. Data and uncertainties were analyzed as in Paper II and Russell *et al.* (1979). The resulting backscatter profile is shown in Fig. 6.

f. Inferred extinction comparison

We converted the dustsonde, filter, and lidar data profiles of Figs. 3–6 to extinction profiles using the conversion ratio values of Fig. A2 and the method of Paper II. (Briefly, at each height, the dustsonde-measured channel ratio value was used to select a model conversion ratio from Fig. A2, and this conversion ratio was multiplied by the measured quantity—number, mass, or backscatter—to yield an extinction estimate.) Resulting extinction profiles are shown in Fig. 7 in comparison to the SAM II and SAGE measurements. Error bars on converted extinction profiles include both measurement and conversion uncertainties; they were derived as in Paper II. Droplet specific gravity values for the mass-to-volume conversion were derived as in Section 2.d (Fig. 1e of Russell and Hamill, 1984).

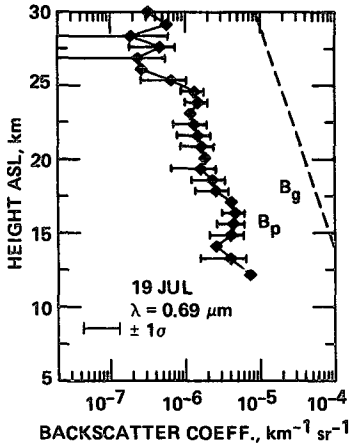

FIG. 6. Particle backscatter B_p, measured by lidar during the Poker Flat experiment. The gas backscatter profile B_g is calculated from radiosonde data.

It can be seen from Fig. 7 that the extinction profiles measured by SAM II and SAGE agree well with those derived from the dustsonde, filter, and lidar measurements. As discussed more fully in Sections 3 and 4, we interpret this agreement as firm evidence that the two satellite sensors were correctly measuring extinction profiles to within the accuracy shown by the satellite error bars.

We have also calculated extinction values from the AWI data by integrating over the (shifted and unshifted) size distributions. The results, shown in Fig. 7, indicate the sensitivity of extinction to small radius shifts—decreases in extinction by factors between 2 and 3 accompany the −15% radius shift. In general, such a uniform radius shift produces AWI-inferred extinction values that are somewhat smaller than the other values. However, note that AWI-inferred extinction for 18 July (Farlow *et al.*, 1981; their Table 1) was much larger than on surrounding days; hence a −13% radius shift for all four days produced a four day *average* extinction value in good agreement with the satellite results. (We have not shown 18 July results because no satellite data are available for that day.) Because the satellite extinction and filter mass values do not show the large (factor of ~3) day to day variability exhibited by the AWI-inferred extinction, it appears that much of the AWI variability is caused by small errors in radius, plus the considerable sampling error for the largest particles ($r > 0.4$ μm), which are very few in number but contribute much of the total mass

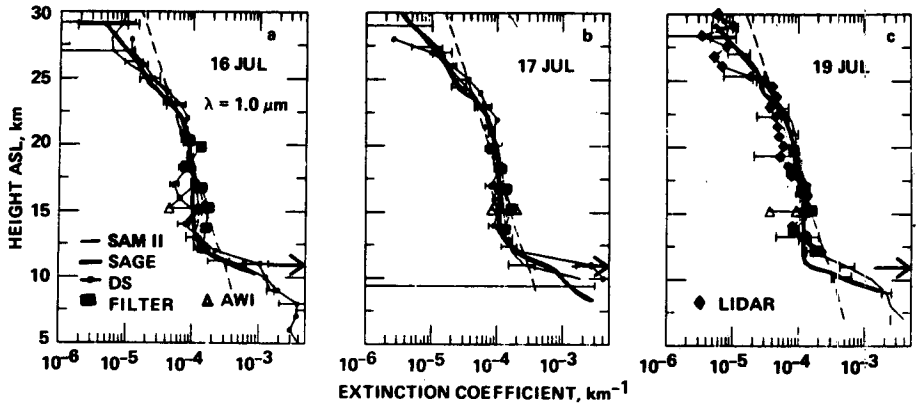

FIG. 7. Comparison of extinction profiles measured by SAM II and SAGE with those derived from dustsonde (DS), filter, lidar and Ames wire impactor (AWI) measurements. For each horizontal pair of AWI data points, the point on the left results from reducing all particle radii by 15%.

and the extinction at the 1.0-μm wavelength. [Filter mass values for 18 July (Gandrud and Lazrus, 1981; their Fig. 1) are essentially the same as on the other days.]

3. Discussion

The above results show excellent agreement between the measurements made by SAM II, SAGE, dustsondes, filters, and lidar. Small negative radius shifts in AWI size distributions improve agreement with dustsonde-measured $N_{0.15}$ values at 15.2 km, but the same radius shift (−15%) reduces mass and extinction values to less than the filter and satellite measurements at the same height. Particle number sampling errors for the largest particles are a possible significant source of error that has not been fully analyzed here. Further experiments and analyses are being conducted to resolve these questions (Ferry, 1982, personal communication).

Thus far we have not shown results from the polar nephelometer (Grams, 1981; see our Table 1) flown at Poker Flat. This instrument measures scattering phase functions, $P(\theta)$, from which one can calculate the scattering asymmetry parameter

$$g \equiv \int_0^{180} P(\theta) \cos\theta \sin\theta d\theta. \qquad (2)$$

Values measured by Grams (1981), for the nephelometer wavelength 0.633 μm, ranged from 0.4 to 0.6, with a mean value of 0.49 ± 0.07, and a slow decrease with height (g = 0.55 at 10.7 km; g = 0.41 at 12.8 km).

These values are in good agreement with a balloon-borne photometer inference by Ackerman *et al.* (1981), which yielded g = 0.45 to 0.62 for a wavelength of 0.650 μm. However, as pointed out by Grams, these values are systematically less than the value of about 0.7 obtained from many stratospheric aerosol models. The model value of 0.7 is often used to calculate radiative effects of the stratospheric aerosol (e.g., Pollack *et al.*, 1981). We note that asymmetry parameter values of 0.7 are also obtained from the model size distributions of Fig. 1 (when the distributions are constrained to yield observed channel-ratio values), as well as from the wire impactor size distributions in Fig. A2. This is a significant discrepancy that needs to be resolved. Grams (1981) has suggested that particle asphericity or nonhomogeneity, not accounted for in the Mie calculations of g, may explain the discrepancy. However, there is much evidence that such asphericities and inhomogeneities are small (e.g., Farlow *et al.*, 1981, and references cited in Paper I). Moreover, the success of spherical, homogeneous particle models in relating lidar, dustsonde, satellite, and filter measurements (e.g., Swissler *et al.*, 1982; Papers I and II; this paper) indicates that they should not be abandoned without strong cause.

4. Summary and conclusions

The large experiment at Poker Flat yielded many areas of agreement and pinpointed some areas of disagreement that require further study. The foremost result is the good agreement of SAM II and SAGE extinction profile measurements, both with each other and with extinction profiles derived from dustsonde, filter, and lidar measurements by using an optical model. The optical model uses refractive indices consistent with the latest picture of stratospheric aerosol composition and temperature (Russell and Hamill, 1984), and size distribution functions constrained to agree with current or recent dustsonde channel ratio measurements. The model is also consistent with the absorption and size distribution measurements made at Poker Flat. From the agreement obtained in the experiment, we conclude that the SAGE extinction measurements are indeed valid, at least for the background-type conditions present during the Poker Flat experiment. The same conclusion was reached for SAM II in Paper II.

The areas of disagreement concerned the polar nephelometer and wire impactor. Polar nephelometer-measured scattering asymmetry factors are significantly smaller than values obtained from Mie-scattering calculations assuming either model or impactor-measured size distributions. For the wire impactor, flattening of impacting particles and other difficulties in assigning an absolute radius scale yield radius uncertainties of ±8% to ±20% (for 95% confidence); this can lead to considerably larger uncertainties in mass, extinction, and numbers of particles larger than fixed size cutoffs (Gras and Ayers, 1979; Gras and Laby, 1981; Farlow *et al.*, 1981). These larger uncertainties result from the steepness of the particle size distribution in the radius region that contributes most to $N_{0.15}$, $N_{0.25}$, extinction, and mass. Another possible difficulty is sampling error for the largest particles ($r > 0.4$ μm), which are few in number but contribute most of the extinction and mass.

In pointing out the above difficulties with impactor measurements, we wish to emphasize the essential nature of these measurements to stratospheric aerosol research in general, and to comparative experiments in particular. Impactors, in general, are the only operational stratospheric sensors that return samples for analyses of particle shape, physical state, composition, and size distribution over a wide radius range. This paper has attempted to derive secondary quantities ($N_{0.15}$, $N_{0.25}$, mass, extinction) that the impactors do not measure directly; not surprisingly, the uncertainties in the derived quantities exceed those of sensors that measure these properties more directly, or with specially optimized designs. Whereas it is important to recognize the uncertainties in the wire impactor secondary quantities, it is equally important that one not lose sight of the unique information on particle shape, physical state, and composition that impactors can yield directly.

Acknowledgments. This research was supported by the National Aeronautics and Space Administration through Contracts NAS1-14314, NAS1-14933, NAS1-16393, and others. William Fuller led the airborne lidar measurements. We are grateful to Bruce Gandrud and Alan Lazrus for discussions of filter data and uncertainties; to Verne Oberbeck, Neil Farlow, Guy Ferry, and Dennis Hayes for discussions of wire impactor measurements; and to Gerald Grams for discussions of scattering asymmetry factors.

APPENDIX

Consistency of Optical Model with Poker Flat Measurements and with Size-Distribution-Independent Approximations

1. Refractive indices

The Poker Flat aerosol absorption measurements of Ogren *et al.* (1981; see their Table 1) yield a most-probable value for singlescattering albedo ω (ratio of particle scattering to extinction) of about 0.985, with an uncertainty range extending from 0.96 to 1.00. (The upper limit is set by the definition of single scattering albedo; measurement uncertainties in fact extend slightly above 1.0.) The inner stratospheric model refractive indices of Fig. 1 (main text), being purely real, yield single scattering albedo values of 1.0. Because this is within the uncertainty range of the Ogren *et al.* measurements, there is no definite conflict between the model and the measurements.

Nevertheless, because the measurements suggest that some absorption may be occurring, it would be useful to explore the implications of an ω value of 0.985 (or less) for model refractive indices and conversion ratios. Unfortunately, a means for doing this is not clear. As Ogren *et al.* note, any absorption is probably caused by small impurities (e.g., graphitic carbon), which are probably not uniformly dissolved in the aerosol droplets. Thus, increasing the whole-droplet imaginary refractive index to yield model single scattering albedos between 0.96 and 1.0 may yield a poor representation of the actual effects of the impurities, especially on lidar backscattering. A more accurate procedure would be to model a two-component system, with a non-absorbing acid/water solution matrix containing small absorbing impurities (Ackerman and Toon, 1981). However, this would be a very difficult process, and uncertainties regarding the nature and position of the absorbing material could yield ambiguous results. For these reasons, but primarily because the model refractive indices fall within the uncertainty range of the absorption measurements, we retain the purely real refractive indices for use in this paper.

2. Size distributions

Within the inner stratospheric layer (Fig. 1, main text) our modeling procedure parameterizes size distributions in terms of dustsonde channel ratio (i.e., $N_{0.15}/N_{0.25}$, where N_x is the number of particles with a radius larger than x μm). A major reason for this procedure is that complete size distribution measurements are not available at most heights in most validation experiments, whereas dustsonde channel ratio profile measurements are more frequently available; moreover, a large data base exists from which channel ratio can be estimated (Hofmann *et al.*, 1975; Hofmann and Rosen, 1977, 1981). Thus, parameterization in terms of channel ratio is useful if knowledge of channel ratio constrains conversion ratios (e.g., extinction-to-number, extinction-to-backscatter) to a relatively small range of values. Paper I and Russell and Hamill (1984) showed that this was the case for the nine families of *model* size distributions used in the inner stratospheric layer (e.g., extinction-to-number ratios for a given channel ratio varied by only ±23% of the mean, provided that the channel ratio was in the commonly measured range of 2.5 to 10). The November 1978 Sondrestrom experiment did not yield any directly

measured size distributions other than the two-channel dustsonde data, so this result could not be tested with actual measurements.

For the Poker Flat experiment, size distributions were determined by electron microscope analyses of samples collected on wire impaction surfaces (Farlow *et al.*, 1981; Oberbeck *et al.*, 1981). We will use these data in two ways to test the validity of parameterization by $N_{0.15}/N_{0.25}$. First we will compare the wire impactor-measured size distributions, classified by $N_{0.15}/N_{0.25}$, with model size distributions similarly classified. Later (Section 3) we will compare conversion ratios calculated for the measured size distributions with model conversion ratios for the same channel ratio values.

Figure A1 shows the size distribution comparison. To make the comparison, all size distributions have been normalized to yield a single value (1 cm^{-3}) for $N_{0.15}$, because only *relative* size distributions are of concern to the model (i.e., the model is used to derive only *ratios* of optical or physical properties, not absolute values). Curves without symbols show the envelope of the nine *model* size distribution families for selected small ranges of channel ratio, $N_{0.15}/N_{0.25}$. (For plots showing the full size distributions for all families, see Fig. 2 of Paper I.) Curves with symbols show the normalized AWI-*measured* distributions, each plotted in the frame appropriate to the measured value of $N_{0.15}/N_{0.25}$. It can be seen that the distributions measured by the AWI lie almost completely within the corresponding model envelopes, and that excursions above or below a model envelope are, with one exception, accompanied by excursions in the opposite direction for nearby radii; these opposite excursions tend to cancel the original excursions when size distributions are integrated over radius. (See Section 3 of this Appendix for verification of this point.) The one exception is the near-tropopause measurement at 12.2 km (Fig. A1b). Note that in this case, for radii larger than about 0.5 μm, the measurement exceeds the model envelope. Although this is but a single case and measurement uncertainties are considerable (see Fig. 1 of Farlow *et al.*, 1981), it is in accord with the behavior noted in Paper I: Size distributions near the base of the inner stratospheric layer and in the tropopause layer have a large particle tail that is underestimated by the inner stratospheric models. (The base of the inner stratospheric layer is 2 km above the tropopause, or at ~13 km for the Poker Flat measurements; see Fig. 1 of main text). Whereas the *number* of particles in this tail is small enough to have little or no impact on $N_{0.15}$, $N_{0.25}$ and $N_{0.15}/N_{0.25}$, the relatively large size of the particles can contribute significantly to mass and to extinction and backscatter at wavelengths of 1.0 and 0.69 μm.

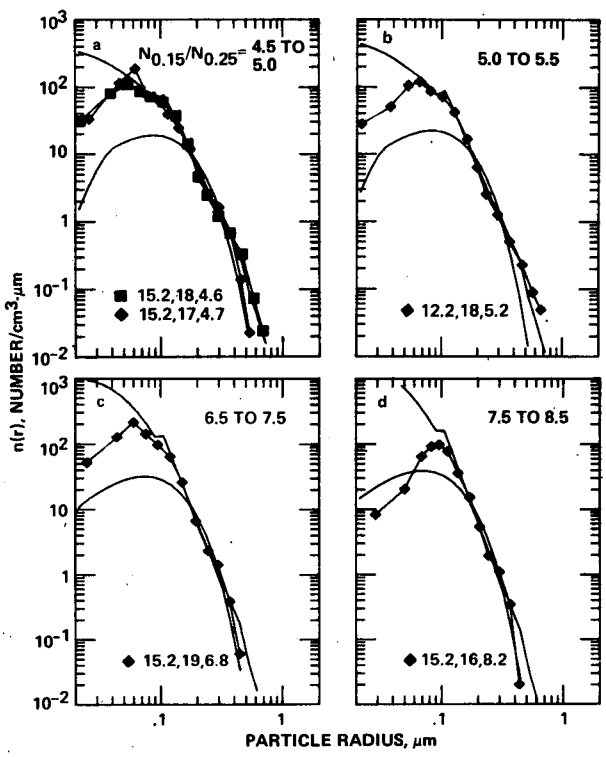

FIG. A1. Comparison of envelopes of model relative size distributions (smooth curves) with Ames wire impactor-measured distributions (symbols) for corresponding channel ratio values ($N_{0.15}/N_{0.25}$). Numbers after symbol legends give measurement altitude (km), day (July 1979) and channel ratio.

As Farlow *et al.* (1981) noted, there are uncertainties concerning the radii assigned to the wire-impactor particle number data points in Fig. A1. These uncertainties are caused by the need to reconstruct from flattened impacted droplets the radii of the original unimpacted spheres, and by other experimental and instrumental constraints. As is shown in Sections 3 and 4 (main text), comparisons suggest that the radii of the AWI data points in Fig. A1 are too large by ~5–15% or more. Therefore, we have repeated the Fig. A1 analysis with the radii of all AWI data points shifted by −15%. In this process, $N_{0.15}/N_{0.25}$ values also change. The results (not shown for brevity) are very similar to those of Fig. A1. That is, the shifted AWI size distributions fall almost completely within the corresponding model envelopes, with excursions above or below the envelopes accompanied by opposite nearby excursions that tend to cancel when distributions are integrated over radius. This cancellation is verified in Section A.3 for both shifted and unshifted AWI distributions.

3. Conversion ratios

Paper I explained the procedure for computing ranges, means, and standard deviations of conversion ratios using model refractive indices and size distribution families. Russell and Hamill (1984; their Fig. 4) showed that inner stratospheric conversion ratios for the new refractive index set (Fig. 1, main text) are very similar to conversion ratios for the Paper I set. Figure A2 repeats the Russell and Hamill model results for the new refractive index set and compares them

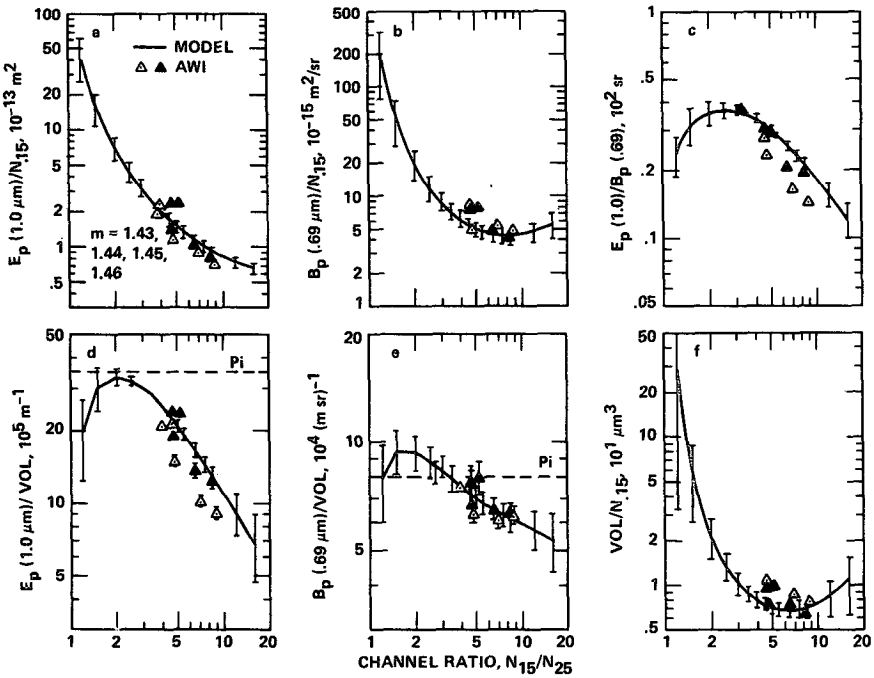

FIG. A2. Conversion ratios for inner stratospheric model size distributions (solid curves) and for size distributions measured by the Ames wire impactor (AWI, symbols). Solid symbols are for the unshifted AWI size distributions; open symbols are for the AWI distributions shifted in radius by −15%. All calculations for model distributions and AWI assume the refractive index set 1.43, 1.44, 1.45, 1.46. Horizontal dashed lines labeled Pi in frames d and e are the size-distribution-independent results of Pinnick *et al.* (1980); they assume $m = 1.422\text{–}2 \times 10^{-7}i$ ($\lambda = 1.0$ μm) and $m = 1.428\text{–}2 \times 10^{-8}i$ ($\lambda = 0.69$ μm).

to conversion ratios computed by combining the AWI relative size distributions of Fig. A1 with the same refractive index set (Fig. 1, main text). Also shown are results obtained with the AWI distributions shifted in radius by −15%. As expected from the good agreement between the model and measured relative size distributions shown in Fig. A1, the impactor-derived conversion ratios (for both shifted and unshifted size distributions) agree well (i.e., to within ~30% or better) with the inner stratospheric model curves. Although the disagreement between model curves and AWI-derived data points in some cases exceeds the model error bars ($\pm 1\sigma$), this disagreement may not be significant because the error bars on the AWI points shown here do not include effects of size distribution measurement uncertainty. (They give only the standard deviation of results for the refractive index set 1.43, 1.44, 1.45, 1.46.) The question of AWI size distribution measurement accuracy is discussed further in Sections 2 and 3 (main text).

Recently Pinnick *et al.* (1980) presented an approximation that yields extinction-to-volume and backscatter-to-volume ratios that are independent of size distribution (and hence of $N_{0.15}/N_{0.25}$). Their results,

$$E_p\ (1.0\ \mu\text{m})/\text{Vol} = 3.5 \times 10^6\ \text{m}^{-1}, \quad \text{(A1)}$$

$$B_p\ (0.69\ \mu\text{m})/\text{Vol} = 8.0 \times 10^4\ \text{m}^{-1}\ \text{sr}^{-1}, \quad \text{(A2)}$$

are indicated by the dashed horizontal lines in Figs. A2d,e. Note that, for E_p (1.0 μm)/Vol (Fig. A2d), the size distribution-independent approximation exceeds the mean results of detailed calculations for all inner stratospheric size distributions, regardless of $N_{0.15}/N_{0.25}$ value.

The reason for this discrepancy is not the slight difference between the room-temperature refractive index ($1.422\text{–}2 \times 10^{-7}i$) assumed by Pinnick *et al.* (1980) and the low temperature values (1.43 to 1.46) assumed here. (In fact, the use of a common refractive index value slightly increases the discrepancy shown—see Fig. 4d of Russell and Hamill, 1984.) Rather, the reason is the relative lack of large particles ($r \geq 0.5$ μm) in inner stratospheric background size distributions. Specifically, the method of Pinnick *et al.* approximates extinction efficiency by a linear function of r in the range $r = 0\text{–}0.9$ μm. For the refractive indices and wavelengths of interest here, the linear approximation exceeds the actual extinction efficiency for all $r < 0.5$ μm (small particles) and underestimates it for $0.5 < r \leq 0.9$ μm (large particles; see Fig. 1 of Pinnick *et al.*). Because particles with $r > 0.5$ μm contribute very little to total extinction for inner stratospheric size distributions (see Fig. 6 of Paper 1), these larger particles are unable to correct for the overestimation that results from the linear approximation at

$r < 0.5$ μm. For backscatter, this small-particle underestimation does not occur (see Figs. 4 and 5 of Pinnick *et al.*), and the size distribution-independent approximation is a more accurate simplification.

REFERENCES

Ackerman, M., C. Lippens and C. Muller, 1981: Stratospheric aerosol properties from earth limb photography. *Nature,* **292,** 587–591.

Ackerman, T. P., and O. B. Toon, 1981: Absorption of visible radiation in atmospheres containing mixtures of absorbing and nonabsorbing particles. *Appl. Opt.,* **20,** 3661–3667.

Bevington, P. R., 1969: *Data Reduction and Error Analysis for the Physical Sciences.* McGraw-Hill, 336 pp.

Biggs, E. K., 1975: Stratospheric particles. *J. Atmos. Sci.,* **32,** 910–917.

——, 1976: Size distribution of stratospheric aerosols and their variations with altitude and time. *J. Atmos. Sci.,* **33,** 1080–1086.

Chuan, R. L., 1970: An instrument for the direct measurement of particle mass. *J. Aerosol Sci.,* **1,** 111–114.

Farlow, N. H., V. R. Oberbeck, D. S. Colburn, G. V. Ferry, H. Y. Lem and D. M. Hayes, 1981: Comparison of stratospheric aerosol measurements over Poker Flat, Alaska, July, 1979. *Geophys. Res. Lett.,* **8,** 15–17.

Gandrud, B. W., and A. L. Lazrus, 1981: Measurements of stratospheric sulfate mixing ratio with a multi-filter sampler. *Geophys. Res. Lett.,* **8,** 21–22.

Grams, G. W., 1981: *In-situ* measurements of scattering phase functions of stratospheric aerosol particles in Alaska during July 1979. *Geophys. Res. Lett.,* **8,** 13–14.

Gras, J. L., and G. P. Ayers, 1979: On sizing impacted sulfuric acid aerosol particles. *J. Appl. Meteor.,* **18,** 634–638.

——, and C. G. Michael, 1979: Measurement of the stratospheric aerosol size distribution. *J. Appl. Meteor.,* **18,** 855–860.

——, and J. E. Laby, 1981: Southern hemisphere stratospheric aerosol measurements, 3. Size distribution 1974–1979. *J. Geophys. Res.,* **86,** 9767–9775.

Hayes, D., K. Snetsinger, G. Ferry, V. Oberbeck and N. Farlow, 1980: Reactivity of stratospheric aerosols to small amounts of ammonia in the laboratory environment. *Geophys. Res. Lett.,* **7,** 974–976.

Hofmann, D. J., and J. M. Rosen, 1977: Balloon observations of the time development of the stratospheric aerosol event of 1974–75. *J. Geophys. Res.,* **82,** 1435–1440.

——, and ——, 1981: On the background stratospheric aerosol layer. *J. Atmos. Sci.,* **38,** 168–181.

——, ——, T. M. Pepin and R. G. Pinnick, 1975: Stratospheric aerosol measurements. I: Time variations at northern midlatitudes. *J. Atmos. Sci.,* **32,** 1446–1456.

McCormick, M. P., P. Hamill, T. J. Pepin, W. P. Chu, T. J. Swissler and L. R. McMaster, 1979: Satellite studies of the stratospheric aerosol. *Bull. Amer. Meteor. Soc.,* **60,** 1038–1046.

——, W. P. Chu, L. R. McMaster, G. W. Grams, B. M. Herman, T. J. Pepin, P. B. Russell and T. J. Swissler, 1981: SAM II aerosol profile measurements, Poker Flat, Alaska, July 16–19, 1979. *Geophys. Res. Lett.,* **8,** 3–4.

Oberbeck, V. R., N. H. Farlow, G. V. Ferry, H. Y. Lem and D. M. Hayes, 1981: A study of stratospheric aerosol maturity. *Geophys. Res. Lett.,* **8,** 19–20.

Ogren, J. A., N. C. Ahlquist, A. D. Clarke and R. J. Charlson, 1981: Measurements of the absorption coefficient of stratospheric aerosols. *Geophys. Res. Lett.,* **8,** 9–12.

Pinnick, R. G., S. G. Jennings and P. Chylek, 1980: Relationships between extinction, absorption, backscattering, and mass content of sulfuric acid aerosols. *J. Geophys. Res.,* **85,** 4059–4066.

Pollack, J. B., O. B. Toon and D. Wiedman, 1981: Radiative properties of the background stratospheric aerosols and implications for perturbed conditions. *Geophys. Res. Lett.,* **8,** 26–28.

Russell, P. B., and P. Hamill, 1984: Spatial variation of stratospheric aerosol acidity and model refractive index: Implications of recent results. *J. Atmos. Sci.,* **41,** 1781–1790.

——, T. J. Swissler and M. P. McCormick, 1979: Methodology for error analysis and simulation of lidar aerosol measurements. *Appl. Opt.,* **18,** 3738–3799.

——, W. Viezee, R. D. Hake, W. P. Chu, J. M. Livingston and T. J. Pepin, 1981a: Satellite correlative measurements of the stratospheric aerosol. I: An optical model for data conversions. *J. Atmos. Sci.,* **38,** 1279–1294.

——, M. P. McCormick, T. J. Swissler, W. P. Chu, J. M. Livingston, W. H. Fuller, J. M. Rosen, D. J. Hofmann, L. R. McMaster, D. C. Woods and T. J. Pepin, 1981b: Satellite and correlative measurements of the stratospheric aerosol. II: Comparison of measurements made by SAM II, dustsondes and an airborne lidar. *J. Atmos. Sci.,* **38,** 1295–1302.

Steele, H. M., and P. Hamill, 1981: Effects of temperature and humidity on growth and optical properties of sulfuric acid-water droplets in the stratosphere. *J. Aerosol. Sci.,* **12,** 517–528.

Swissler, T. J., P. Hamill, M. Osborn, P. B. Russell and M. P. McCormick, 1982: A comparison of lidar and balloon-borne particle counter measurements of the stratospheric aerosol 1974–1980. *J. Atmos. Sci.,* **39,** 909–916.

Toon, O. B., and J. B. Pollack, 1976: A global average model of atmospheric aerosols for radiative transfer calculations. *J. Appl. Meteor.,* **15,** 225–246.

——, R. P. Turco, R. Whitten and P. Hamill, 1981: Implications of stratospheric aerosol measurements for models of aerosol formation and evolution. *Geophys. Res. Lett.,* **8,** 23–25.

Woods, D. C., 1979: Measurement of particle aerosol mass concentration using a piezoelectric crystal microbalance. *Aerosol Measurement.* D. A. Lundgren *et al.,* Eds., University of Florida Press, 119–142.

Yue, G. K., and A. Deepak, 1981: Modeling of growth and evaporation effects on the extinction of 1.0-μm solar radiation traversing stratospheric sulfuric acid aerosols. *Appl. Opt.,* **20,** 3669–3675.